Original Research Article

International journal of spray and combustion dynamics

International Journal of Spray and Combustion Dynamics
2017, Vol. 9(4) 310–329

DOI: 10.1177/1756827717703577
journals.sagepub.com/home/scd

SAGE

Numerical analysis of the dynamic flame response of a spray flame for aero-engine applications

Alessandro Innocenti[1], Antonio Andreini[1], Bruno Facchini[1] and Antonio Peschiulli[2]

Abstract

Incoming standards on NO_x emissions are motivating many aero-engine manufacturers to adopt the lean burn combustion concept. One of the most critical issues affecting this kind of technology is the occurrence of thermo-acoustic instabilities that may compromise combustor life and integrity. Therefore the prediction of the thermo-acoustic behaviour of the system becomes of primary importance. In this paper, the complex interaction between the system acoustics and a turbulent spray flame for aero-engine applications is numerically studied. The dynamic flame response is computed exploiting reactive URANS simulations and system identification techniques. Great attention has been devoted to the impact of liquid fuel evolution and droplet dynamics. For this purpose, the GE Avio PERM (partially evaporating and rapid mixing) lean injection system has been analysed, focussing attention on the effect of several modelling parameters on the combustion and on the predicted flame response. A frequency analysis has also been set up and exploited to obtain even more insight on the dynamic flame response of the spray flame. The application is one of the few in the literature where the dynamic flame response of spray flames is numerically investigated, providing a description in terms of flame transfer function and detailed information on the physical phenomena.

Keywords

Flame transfer function, system identification, liquid fuel, thermo-acoustic behaviour, dynamic flame response, spray flame, lean burn

Date received: 27 September 2016; accepted: 13 March 2017

1. Introduction

One of the main targets for the next generation of civil aero-engines is the abatement of engine pollutant emissions, in particular NO_x, to meet the stringent regulations to be implemented in the near future. The most prominent way to achieve compliance is represented by lean burn technology.

Huge efforts have therefore been put into developing injection strategies, i.e. lean direct injection (LDI) systems, that create a lean burning mixture directly inside the combustion chamber by improving the rate of spray evaporation and fuel air mixing.

An example of such a technology is the so-called PERM (partially evaporating and rapid mixing) injector developed by GE Avio. The PERM injector, investigated in this paper, is a double swirler airblast atomizer developed to achieve partial evaporation inside the inner duct and rapid mixing within the combustor, optimizing the location and stability of the flame. Further details about the PERM injector can be found in papers by Kern et al. and Andreini et al.[1,2] Other studies on the flow field generated by a PERM injector and its interaction with the cooling system at combustor walls can be found in Andreini et al. and Mazzei et al.[3,4]

One of the most critical issues of lean combustion technology is the possible occurrence of combustion

[1]Department of Industrial Engineering, University of Florence, Italy
[2]Combustor Technology, GE Avio S.r.l., Rivalta di Torino, Italy

Corresponding author:
Alessandro Innocenti, Department of Industrial Engineering, University of Florence, 50139 - Via S. Marta 3, Florence, Italy.
Email: alessandro.innocenti@htc.de.unifi.it, antonio.andreini@unifi.it

instabilities related to a coupling between pressure oscillations and unsteady heat release. Such instabilities may damage the combustor's components and limit the range of stable operating conditions. Therefore, the prediction of the thermo-acoustic behaviour of the system from the early design phase on becomes of primary importance.

For this a deep understanding and an accurate description of the flame and of the main driving mechanisms that affect its dynamics are necessary. The flame can be considered a black-box input–output system with the driving mechanisms as input and the unsteady heat release as output. For sufficiently small levels of perturbation the flame response can be considered linear. Each input can be related to the output through a so-called flame transfer function (FTF). In a real combustion system, together with acoustic perturbations, equivalence ratio fluctuations can also contribute to the dynamic response of the flame. For spray flames the situation is even more complex due to the effects that acoustic perturbations may have on specific processes such as atomization, evaporation and successive evolution and mixing. The interaction of the acoustic field with the fuel spray can produce periodic variation of the spray shape, droplet size distribution and, in turn, a variation in the evaporative and mixing processes.[5–7] These periodic variations in fuel supply rate and/or periodic variations of the equivalence ratio at the flame location produce heat release oscillations that drive the acoustic field.[8–10] The physical processes involved are very complex and not completely understood with very few investigations available in literature especially for the interaction between acoustics and droplet primary breakup.[11]

Commonly employed simplified FTF formulations are in many cases inadequate to represent the complex physics lying behind the flame dynamic response. Concerning liquid fuel FTFs, Eckstein and Sattelmayer (2006) proposed a formulation for diffusion flames generated by an airblast injection system.[12] The fluctuation of droplet diameter caused by the fluctuation of air velocity is considered the main driving mechanism: assuming a negligible pre-vaporization,[12,13] the heat release rate is directly proportional to the droplet evaporation rate and thus a relation between heat release fluctuations and droplets diameter can easily be found. Eckstein et al. proved that for low-frequency combustion oscillations a quasi-steady description of the airblast atomizer is appropriate and droplet diameter fluctuations can be directly related to air velocity fluctuations at the injection plane.[7] They in fact observed that positive air velocity fluctuation leads to a positive oscillation of the heat release rate because a higher velocity causes a reduction of droplet mean diameter and therefore a greater heat release rate.

In the study by Andreini et al.,[11] the capabilities of different FTF formulations in reproducing the complex PERM generated flame were tested. The thermo-acoustic behaviour of the PERM equipped combustor has been shown to be strongly dependent on operating conditions,[14,15] and simple FTF formulations seem to be inadequate to study the thermo-acoustic stability at several operating conditions.

An attractive alternative way to determine the FTF consists in its computation from computational time series data generated with unsteady computational fluid dynamics (CFD) simulations where the flame dynamics are reproduced. A simulation is performed exciting the system with a carefully designed broadband signal while recording the time series of the system inputs and heat release fluctuations. Exploiting system identification (SI) post-process techniques it is possible to obtain the FTFs relating each input to the output of the system, thus completely characterizing the flame response.

Several applications to laboratory gas flames and to industrial technically premixed gas flames can be found in the literature.[16–24]

Concerning the application to liquid fuels only few studies are present in the open literature. In their investigation, Zhu et al. focussed on the low-frequency oscillation (in the range 50–120 Hz) commonly called 'rumble'.[25] They performed Reynolds-averaged Navier–Stokes (RANS) simulations of a simplified domain and computed the system transfer function by determining the coefficients of an infinite impulse response filter for which the output signal is the downstream heat release rate while the input signal is the inlet flow rate. Information is provided distinguishing two forms of the low-frequency quasi-steady response. In the primary zone the rate of combustion was found to be enhanced when the inlet air velocity is high. On the contrary, near the flame front the rate of combustion strictly depends on the mixture fraction and it is higher when the mixture fraction is close to the stoichiometric value. At higher frequencies the combustion lags this quasi-steady response through simple time-lag laws.

In the present research, a coupled CFD–SI approach based on unsteady RANS (URANS) simulations is used to compute the FTF. The methodology is applied to study a lean spray flame generated by the GE Avio advanced PERM injection system in a laboratory test case. In particular the numerical tools are exploited to carry out sensitivity analyses to several modelling parameters involved in spray combustion simulations. The effects on the combustion process and on the flame shape are analysed to get more information on the system response to acoustic perturbations and its relation with the liquid fuel evolution within the

combustor. The paper is structured as follows: the investigated combustor is presented at first. Then the used numerical models are discussed. Following, the results of preliminary investigations carried out to select the numerical domain, to assess the numerical procedure and to select the proper mesh are presented. The influence of the liquid fuel properties, the chemical mechanism and the wall thermal boundary effects are discussed in the main results section before reporting the main conclusions.

2. Investigated combustor

A scheme of the functioning concept of the GE Avio PERM injector is depicted in Figure 1. The PERM is a double radial co-rotating swirler where liquid fuel is mainly injected by a prefilming airblast scheme.

A film of fuel is generated over the inner surface of the lip that separates the two swirled flows. As the film reaches the edge of the lip primary atomization occurs: fine droplets and rapid mixing are promoted by the two co-rotating swirled flows generated by the double swirler configuration. In order to ensure a stable operation of the lean burn system the airblast injector is coupled with a hollow cone pressure atomizer (pilot injector) located at centre of the primary swirler, which generates a pilot flame to stabilize the combustion process in a configuration usually referred to as 'piloted airblast'. When working at atmospheric conditions the atomizer is operated using the pilot fuel injection only.

The test-rig where the PERM injector was installed is available at TU Munich: it was the object of a specific research in the framework of a European programme named KIAI, where spray flame diagnostics were carried out; for more details, see Gikadi and Sattelmayer.[26] A sketch of the test-rig is reported in Figure 2.

A single PERM injector is installed on the rig and it is fed by an upstream plenum with circular cross section. A highly homogeneous reacting fuel mixture is produced by the PERM injector and a flame is stabilized in the combustion chamber which, differently from the plenum, has a square cross section. The combustion chamber is cooled from the outside using impinging air jets and is followed by an exhaust gas system.

The adopted measurement technique involves the evaluation of the lumped acoustics transfer matrices with the two-source technique according to Munjal and Doige:[27] measurements were obtained for the burner with and without the presence of a flame. A perforated screen is mounted at the rig outlet in order to realize stable conditions for the measurement of the FTF. For further details on the experimental test-rig design, on the used experimental methodology and obtained results the reader is referred to Gikadi.[28]

In the present work, non-dimensional frequencies are represented in terms of Strouhal number (St) considering the gas velocity at the burner outlet and the injector exit diameter. The St range considered in the measurements falls between 0.03 and 0.49. An increment step of 0.006 is considered in the measurements.

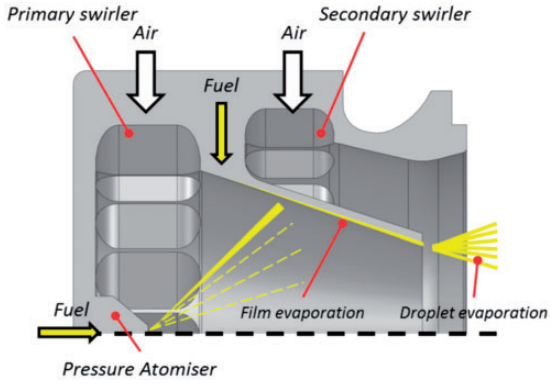

Figure 1. Scheme of the PERM injector.[3]

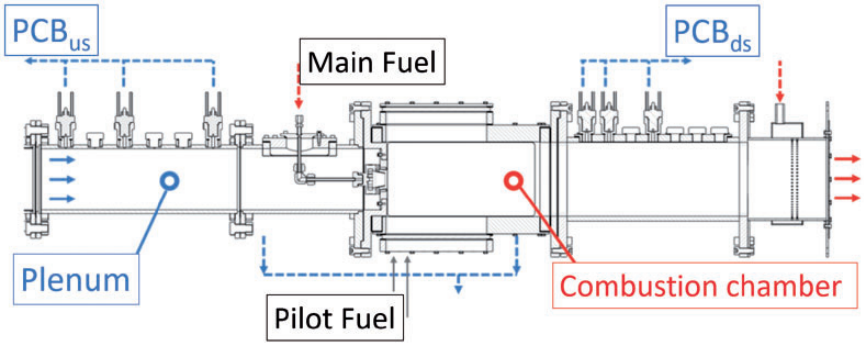

Figure 2. Scheme of the reactive test-rig at TU Munich.[26]

3. Numerical details

3.1. Basics of CFD modelling

Compressible Navier–Stokes equations are solved with the finite volume solver ANSYS Fluent v15.0.7 using a URANS approach, where turbulence was modelled with the $k-\epsilon$ model coupled to scalable wall functions.

3.2. Combustion modelling

Combustion is treated with a flamelet generated manifold (FGM) model. In the FGM model, a two-dimensional manifold is generated by solving a set of laminar one-dimensional flamelets and parametrizing the chemical state and reaction progress space only as function of two control variables, i.e. the mixture fraction Z and the normalized progress variable $c = Y_c/Y_{c,\mathrm{eq}}$. In the present work, the non-normalized Y_c is evaluated from CO and CO_2 species

$$Y_c = Y_{\mathrm{CO}} + Y_{\mathrm{CO_2}} \tag{1}$$

Flamelet equations have been solved using the dedicated tool integrated in ANSYS Fluent v15.0.7. Strained premixed flamelets were evaluated using a skeletal reaction mechanism due to Kundu et al.[29] This scheme, named hereafter JetAk99, is based on a single element surrogate for Jet-A fuel, i.e. $C_{12}H_{23}$, and it counts in total 16 species and 39 reactions. Flamelets are solved for different values of equivalence ratio and scalar dissipation rate. The latter quantity is modelled by the solver as an algebraic function of progress variable and mixture fraction and is not therefore considered as an independent variable of the manifold. In order to take into account the turbulence-chemistry interactions, laminar quantities of the generated manifold are integrated in the pre-processing stage using a presumed probability density function approach (β-PDF) for both mixture fraction and progress variable.[30] Accordingly, the mean source term for the progress variable equation is also modelled by integrating the finite-rate flamelet source term from the flamelet library. In order to properly model diabatic cases with fixed wall temperature, an extra dimension due to the enthalpy gain/loss has been added to the tables, while radiative effects have been neglected.

3.3. Spray modelling

For the spray dynamics and gas–liquid interactions a coupled Eulerian–Lagrangian formulation is used. As already mentioned, in the experimental tests at ambient pressure the fuel is injected at the pilot injector only. However, at low pressure the pilot fuel does not evaporate instantly and the droplets impinge on the lip inner surface, creating a liquid film of fuel, as shown in Figure 1. Following previous experience,[2] the liquid film is not modelled and liquid particles are injected directly from the lip where the primary breakup occurs. A surface injection is realized over a small portion of the lip tip. Particles are introduced with a 0° injection angle and a temperature of 298 K. For the droplet size distribution a Rosin–Rammler PDF was used with a mean droplet size of 6.32 μm and a spread parameter of 2. Models for droplet motion, evaporation and heat transfer are needed to obtain the spray distribution and provide source terms of mass, momentum and energy to the continuous phase, as required by the adopted two-way coupling. For the liquid momentum equation only drag and gravity effects have been accounted for, evaluating the drag coefficient through the hypothesis of spherical not deformable shape as in Morsi and Alexander.[31] Secondary breakup effects have been considered through the well-known Taylor analogy breakup (TAB) model,[32] since the maximum Weber number inside the numerical domain was found to be lower than 100 in all the simulations realized. The dispersion of particles due to turbulence in the fluid phase is included using the random walk model.[33] For the evaporation modelling a uniform temperature model has been used,[34] where the integration of convection contribution on the mass transfer is included exploiting the formulation derived in Sazhin.[35] Properties of the gaseous phase around each droplet have been evaluated through the well-known one/third rule.[36] The influence of constant or temperature-dependent liquid fuel properties was studied, in particular the effect of considering liquid fuel properties constant with temperature or using the property laws reported in Rachner.[37]

3.4. Numerical setup

A simulation time step of 1.0×10^{-5} is chosen in order to have a Courant number below unity in the domain. Liquid fuel particles are tracked with the same time step used for the fluid flow, updating species and energy source terms every time-step. After an initialization period required to flush out the initial conditions and to allow the underlying flow field to develop, the mean values are computed by collecting the time statistics over about four flow-through times.

A second-order scheme is adopted for the spatial discretization except for turbulence related quantities for which a first order upwind is adopted. A bounded second order implicit scheme is used for the time discretization. A coupled solver is used for pressure–velocity coupling.

A specified air mass flow is assigned at the inlet section of the feeding duct that constitutes the plenum. The air is then introduced from the dedicated inlet section in the experimental conditions that is pre-heated and at ambient pressure. At the lateral surfaces periodic boundary conditions are assigned while plenum walls are considered adiabatic. Sensitivity to liner walls thermal treatment is presented in the following sections. Discrete phase reflection condition is imposed at all the walls. At the outlet section, the Fluent non-reflecting boundary condition is assigned to prevent resonances inside the domain which could eventually alter and deteriorate the FTF identification.[38]

ANSYS ICEM-CFD was used to generate hybrid computational meshes (polyhedral with a near wall prismatic layer). The mesh adopted for all the sensitivity analyses was chosen after studying the influence of the mesh refinement on the spray combustion.

The computational costs associated to the realized simulations can be summarized as follows. Simulations were all carried out on a single cluster node counting 16 CPU cores (Intel Xeon E5-2630v1). Calculations with steady boundary conditions required about 5 days for a full convergence of flow variable statistics while runs with inlet acoustic excitation required between 7 and 12 days depending on the considered mesh.

3.5. Flame transfer function computation

Assuming a velocity-sensitive behaviour of the flame dynamics, the integral heat release can be considered mainly driven by acoustic velocity at the injector outlet. For small perturbations the system representing the flame can be considered a linear time-invariant single input–single output (SISO) system. Exploiting the convective nature of the flame response a finite impulse response (FIR) structure can be used to model the flame.[16,39,40]

The computed flame response to normalized acoustics fluctuations represents a discrete data set where the input is $x_n = u'/\bar{u}$, while the output, expressed as the normalized heat release rate fluctuation ($y_n = q'/\bar{Q}$), can be evaluated as follows

$$y_n = \sum_{k=0}^{M} h_k x_{n-k} \tag{2}$$

where M is the 'problem dimension', i.e. the length (in time) of the impulse response, h_k. This should be able to represent the system and, generally, it can be considered as the longest characteristic convective time of the system. Some physical knowledge is then provided to define the FIR model structure. Therefore it should be considered as grey-box model of the flame.[40]

In the present work, the mean particle residence time was chosen, leading to a problem dimension of $M = 524$. The frequency response of the flame, the FTF, can be determined as the Z-transform of the impulse response vector

$$FTF(\omega) = \sum_{k=0}^{M} h_k e^{-i\omega k \Delta t} \tag{3}$$

Therefore the problem consists in the determination of the impulse response from CFD time series. This is accomplished exploiting a non-recursive least square method. The identification is based on the Wiener–Hopf linear least square estimator, which exploits correlation functions between the input and the output of the system (refer to Ljung,[41] for example, for a complete treatment of the SI).

The computed FTF is valid in the low-frequency regime, which is analysed in this work.

After determining the mean values with steady boundary conditions the inlet mass flow rate is excited with a square wave with randomly variable amplitude (RASW) signal. It combines some of the characteristics of a random binary signal and of random noise. The cut-off frequency is defined by the period of the square wave and it is chosen at St 0.5 in the present work. Broad-banding is provided by the variable amplitude. The signal mean is zero and the amplitude varies around it following a Gaussian distribution of imposed variance. Tests on RASW signal showed good features of broad-banding and filtering. The maximum wave amplitude is limited to the 20 % while mean amplitude variation is 10 %. Preliminary tests to verify linearity hypothesis are not reported here. For further details please refer to Andreini et al.[42]

The system is excited for 0.2 s and the data are exported at each time step.

4. Preliminary investigations

4.1. Domain selection

To select the computational domain to perform the main part of the analyses and with the aim of reducing computational costs, two geometries are tested:

- 1/4th sector of the whole domain (compatible with both swirler minimum periodicity of 1/16th and the squared combustion chamber);
- 1/16th of the domain so that only one of the 16 swirler inlet channel is simulated. A far as the combustion chamber is concerned, an axisymmetric tubular combustor is considered with equivalent effective area.

Such preliminary investigation is carried out for perfectly premixed gaseous flame to save computational time.

In Figure 3, the numerical domain and grids used are shown. The resulting number of elements of 1.45×10^6 for the 1/4th domain and 5.2×10^5 for the 1/16th domain. Localized refinements are realized in the swirler section and in the first part of the flame tube where the main reaction rates are expected. A further coarsening is then realized towards the outlet section.

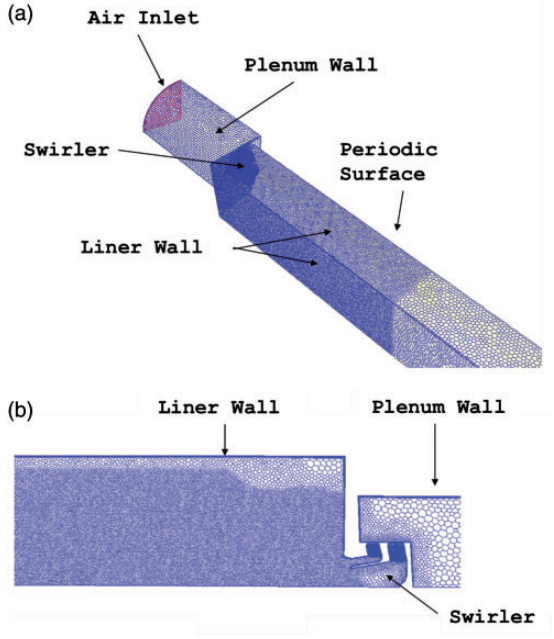

Figure 3. Numerical meshes used for the 1/4th sector domain (a) and for the 1/16th sector domain (b).

From temperature and axial velocity contours in Figure 4 it is possible to see the typical flow field with the high velocity jet region that impinges on the wall and the main recirculation bubble. Similar flame shapes are predicted. In Figure 5, velocity, temperature and product formation rate (PFR) profiles are plotted against the scaled radius. At all the sampled sections a similar behaviour is predicted for both the domains. PFR profiles highlight two main regions of activity at the inner and outer shear layers of the jet. Moving downstream a complete combustion is predicted apart from the region close to the wall where lower temperature levels are observed. It is in this region that the main differences can be observed between the domains: at $x = 0.15$ m the 1/4th shows higher formation rate and lower temperature due to a slower attainment of the equilibrium. In terms of velocity the two cases are practically equal.

From this preliminary investigation only slight differences emerged between the studied domains. Even if this might influence the flame response to the acoustic perturbation, the differences can be considered negligible. Therefore, the 1/16th domain is chosen to carry out the following investigations.

4.2. FTF with perfectly premixed $C_{12}H_{23}$ flame

Before studying a case with liquid fuel injection, the FTF for the perfectly premixed case has been computed on the 1/16th domain to assess and validate the whole CFD–SI procedure.

In Figure 6, the computed FTF of the premixed flame is plotted against the measurement performed for a spray flame. The results are not directly comparable but it is interesting to see the main differences that arise.

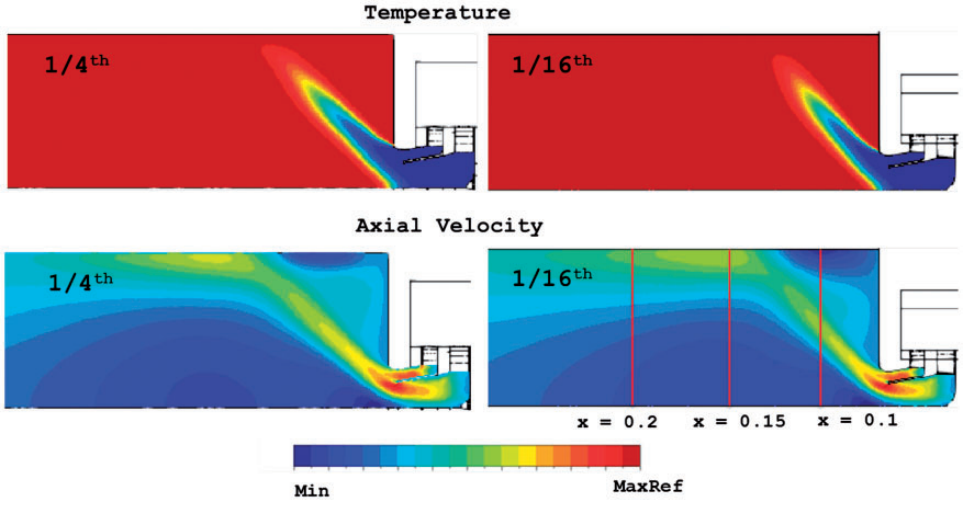

Figure 4. Contours of temperature and axial velocity for the simulated computational domains with different periodicity.

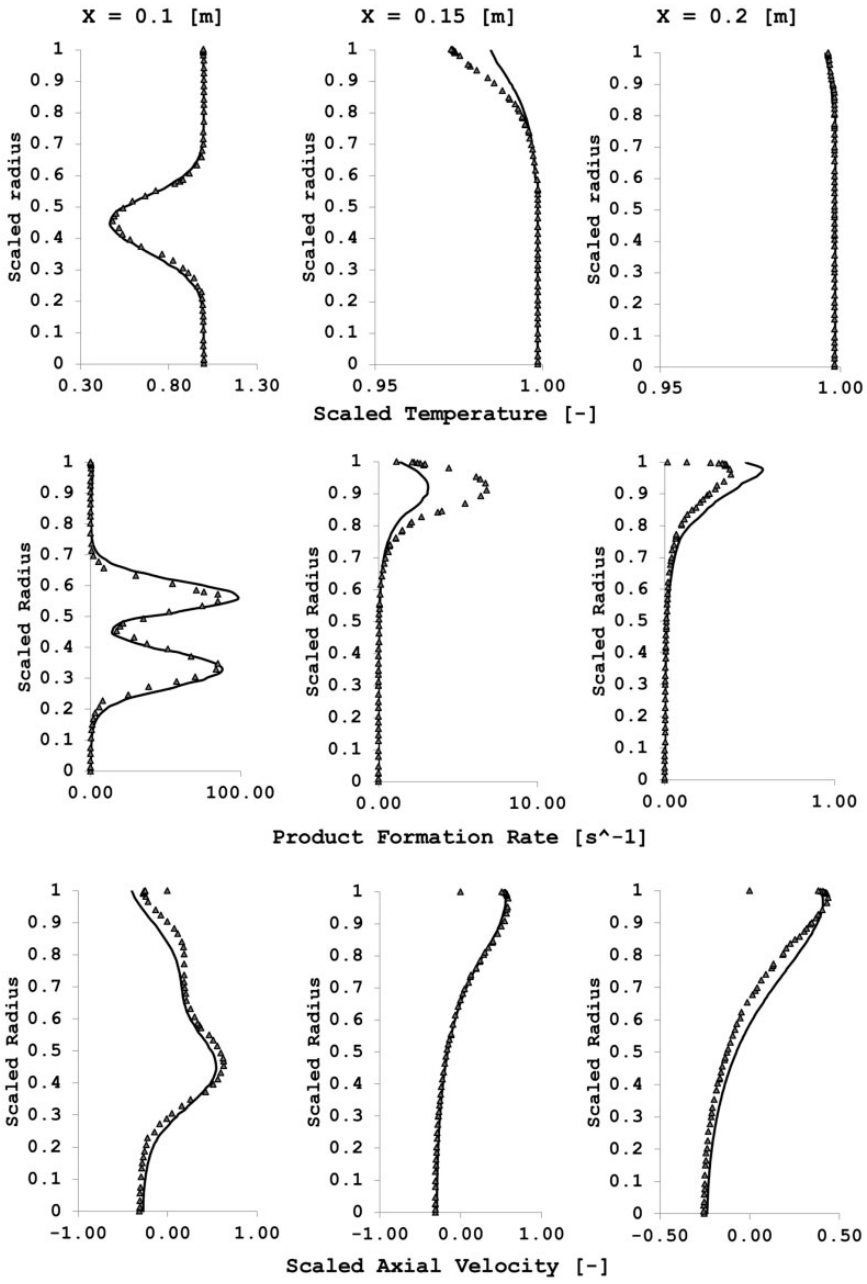

Figure 5. Comparison between scaled temperature, product formation rate and scaled axial velocity profiles obtained for the 1/4th (▲) and the 1/16th (—) domains at three axial locations.

The FTF gain has the typical shape of a premixed flame: the response to acoustic excitation decreases with the frequency showing the low-pass filter behaviour of the flame. The gain tends to values close to the theoretical limit of 1.0 when the frequency tends to 0.0.[43] For low frequencies, i.e. below St = 0.15, the predicted and the experimental FTFs show very different behaviours: the FTF for the premixed flame has a monotonic growing trend with the frequency while the experimental one starts from values exceeding unity at frequencies below St = 0.03 and has a decreasing trend until a minimum is reached at around St = 0.92. A growing trend is then measured to the maximum at around St = 0.184. The frequency of the maximum is close for the two cases.

Comparing the phases a similar trend is observed in the first part of the range of interest. For higher frequencies the premixed flame shows different characteristic time lags.

In the following the dynamic behaviour in case of liquid fuel injection is studied.

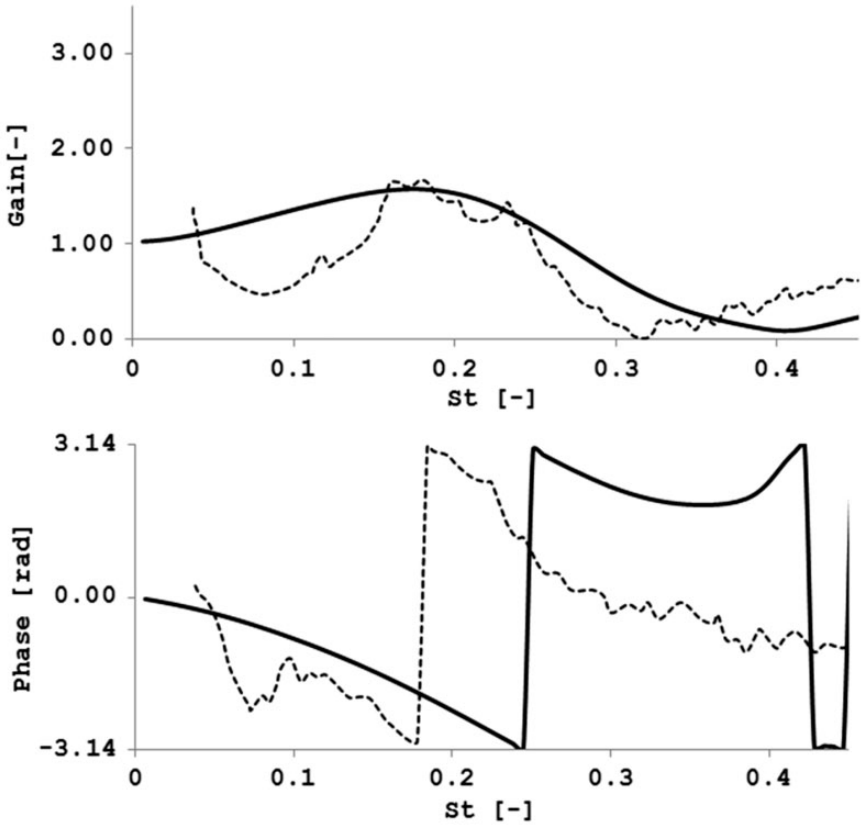

Figure 6. Experimental spray flame FTF (- -); perfectly premixed $C_{12}H_{23}$ flame FTF (—).

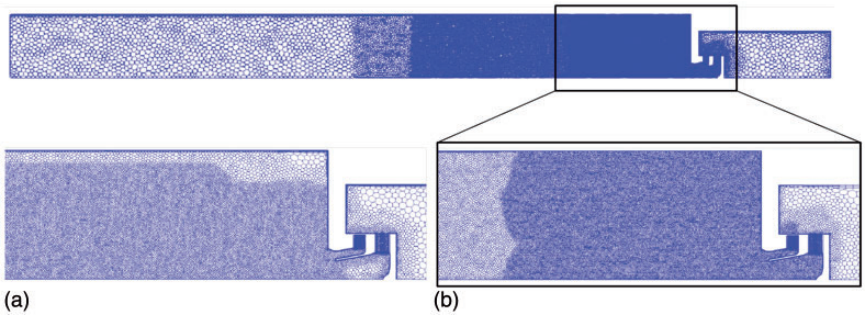

Figure 7. Pictures of the coarse (a) and refined (b) mesh used for the mesh sensitivity analysis.

4.3. Mesh sensitivity

A mesh sensitivity analysis has been carried out to understand the effect of a mesh refinement in the spray region on the combustion process.

The two meshes used in the simulations are depicted in in Figure 7. While the coarser mesh (M1) counts about 5.2×10^5 elements, the finer one (M2) results in 6.2×10^5. A mesh refinement is realized in the first part of the domain, while the last part has been coarsened not to impact in a dramatic way the total number of elements. The element growth rate has been reduced considerably in M2 in all those regions where it is expected the presence of liquid fuel.

In M1, an eight-element layer is present while only two elements are introduced in M2, considering the prismatic layer impact limited for this case studied and allowing a considerable saving in the resulting global number of mesh elements. A localized refinement is realized for M2 in the near wall location where the liquid droplets impinge: the liquid phase evolution is expected to be more faithfully predicted in this zone.

In Figure 8, the results of the two simulations with M1 and M2 are shown. A more confined spray jet with

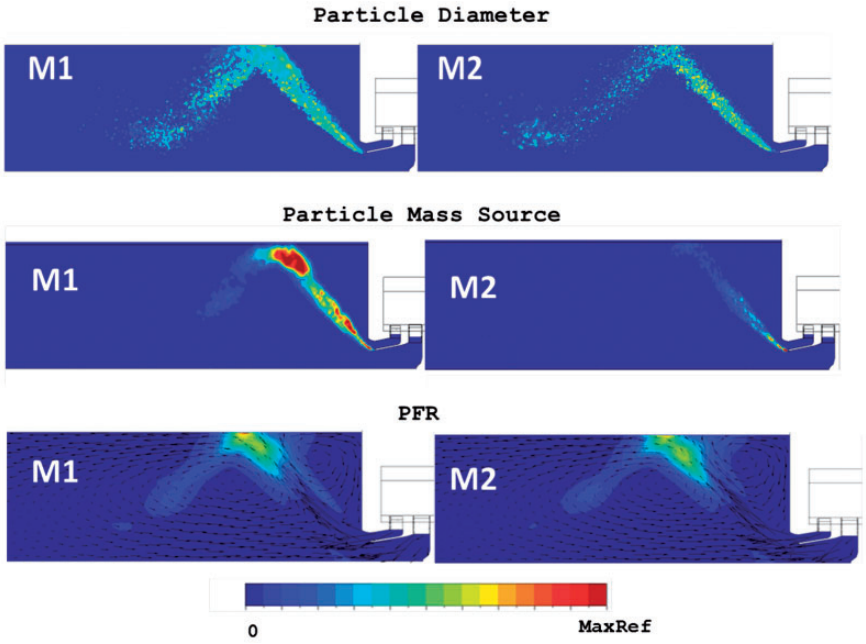

Figure 8. Contours of particles diameters, particle mass source and product formation rate: effect of the mesh refinement.

smaller opening angle is predicted on the finer mesh M2. A limited impact is observed on particles diameter so that the secondary breakup model is supposed to act in a similar way and not being influenced by the mesh size.

In both the cases the injected particles from the lip tip are suddenly trapped by the high velocity jet. Impingement on the liner wall is observed before the particles are reflected. The greatest evaporation rate is observed close to the wall and only a small number of particles is seen after wall reflection.

As far as the particle mass source is concerned, a localized evaporation in the initial region of the spay is predicted on M2. On the coarse mesh a smoother distribution is found. Great mass sources are observed on M1 in the coarse region along the combustor wall. The effect is limited on M2, in a more physical way.

As a consequence of the evaporation pattern PFR shows a single peak at the wall for M1 while a second peak is predicted on M2, closer to the injector. Smaller time lags are expected in the FTF (smaller phase) for M2.

The differences in particles evolution do not heavily impact the flow evolution, as seen in Figure 9. Also, mixture fraction and temperature distributions are similar. Therefore the impact of the mesh refinement is limited to the discussed effects and a similar FTF is expected for the two cases.

The FTF computed with the two meshes are reported in Figure 10. The amplitudes show similar trends. The low frequency behaviour of the measured gain is not represented and both the computed FTFs approach 0.0 when the frequency goes to 0.0. The maximum location is predicted at around $St = 0.11–0.184$. M1 seems to catch better the decreasing trend which follows as well as the minimum gain in the higher frequency range.

However, looking at the phase plot, representative of the time delay between the acoustic fluctuations at the injector exit and the following heat release response, improved results are obtained with the finer mesh M2. Higher time lags are associated with M1, possibly due to the heat release peak predicted slightly downstream in this case, as discussed before.

As for the gain, also the phase does not follow experiments in the low frequency range. Higher time lags seem to characterize the experiments and the specific dynamics is not seen by the model. Therefore the resulting FTF is not representative in this range.

From the mesh sensitivity analysis it is possible to conclude that the amplitude shows similar trends for both the meshes even if M1 seems to follow the amplitude of the experiments. The phase is better represented when the finer mesh is used. Considering this aspect of prime importance, the fine mesh M2 is used to continue the investigation and the sensitivity analyses.

It does not seem worth to further refine the mesh when also considering computational costs and the purpose of the investigations, which is to assess the methodology to numerically compute the FTF for spray flames to understand the effects of the main simulation and modelling parameters. A good compromise is obtained with M2 mesh.

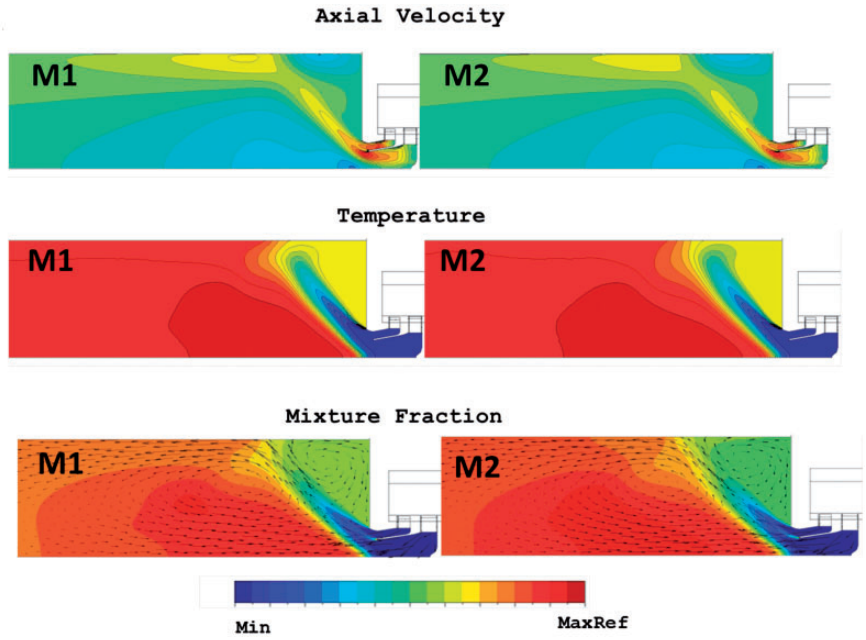

Figure 9. Contours of axial velocity, temperature and mixture fraction obtained with the two meshes.

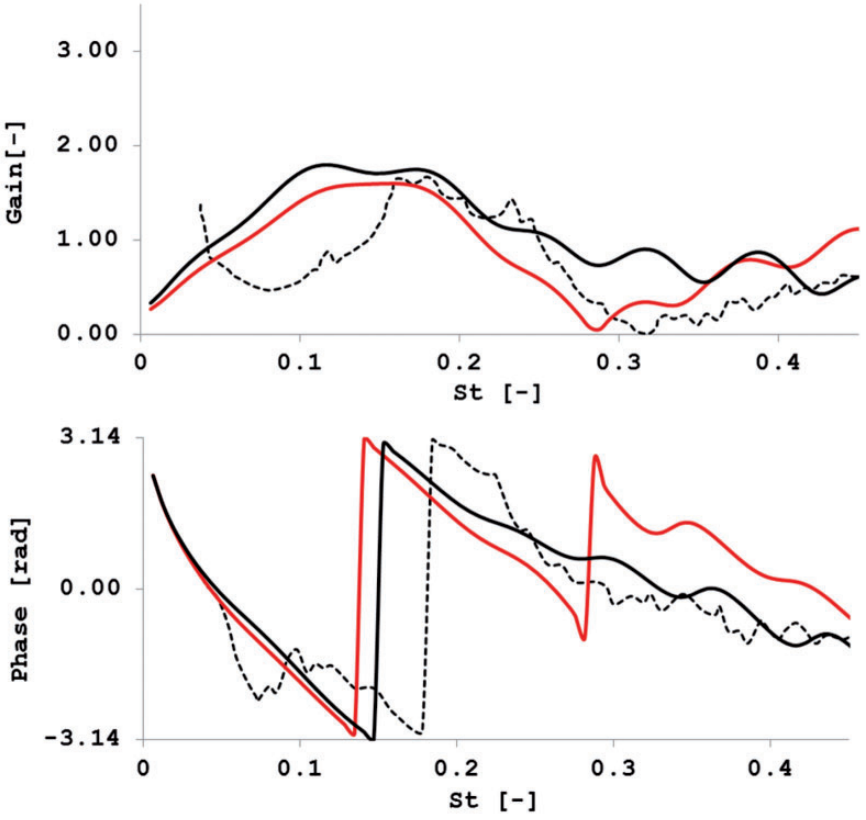

Figure 10. Experimental FTF (- -), FTF computed with M1 (—) and FTF computed with M2 (—).

5. Results

In this section the sensitivity analyses to modelling parameters and their impact on the FTF are presented. Table 1 summarizes the main simulations carried out and the main changes introduced in the numerical model.

5.1. Sensitivity to liquid phase properties

A sensitivity analysis is carried out with respect to the liquid fuel material properties. In particular, the dependency from temperature is included, according to Rachner,[37] for the following properties:

- density;
- viscosity;
- specific heat;
- surface tension.

Table 1. Simulations carried out and main modelling changes introduced.

ID	Liquid prop.	Mechanism	Wall thermal BC
C-Jk-Ad	constant	JetAk99	adiabatic
V-Jk-Ad	variable	JetAk99	adiabatic
V-JkN-Ad	variable	JetAk99N	adiabatic
V-JkN-Tw	variable	JetAk99N	T_w = constant

All the other numerical settings and properties the same used in previous simulations.

Figure 11 shows the mean fields of particle diameter, particle mass source and PFR. In the left column the data for constant liquid properties are shown, the right column shows the results obtained with variable liquid properties. A larger spray cone is predicted and particle diameters decrease. The evaporation rate is enhanced and particles partially evaporate in the first part of the jet. Increased particle mass sources are observed closer to the injection point. Consistently an earlier evaporation leads to a more uniform mixture fraction distribution and smoother temperatures which can be seen in Figure 12. Here again, the constant property results are in the left column.

Concerning the product formation (Figure 11) the reaction is moved upstream and a higher peak appears before the liner wall is reached. The intensity of the reaction after wall impingement and in the inner recirculation is instead reduced in the simulation with the variable liquid properties.

The computed FTF is shown in Figure 13 (red curve). The predicted gain assumes higher values, in line with the more intense PFR observed. The peak location is at the same frequency as the experiments but with twice the values. A relative minimum is obtained at St = 0.3 but with a further increase on the frequency

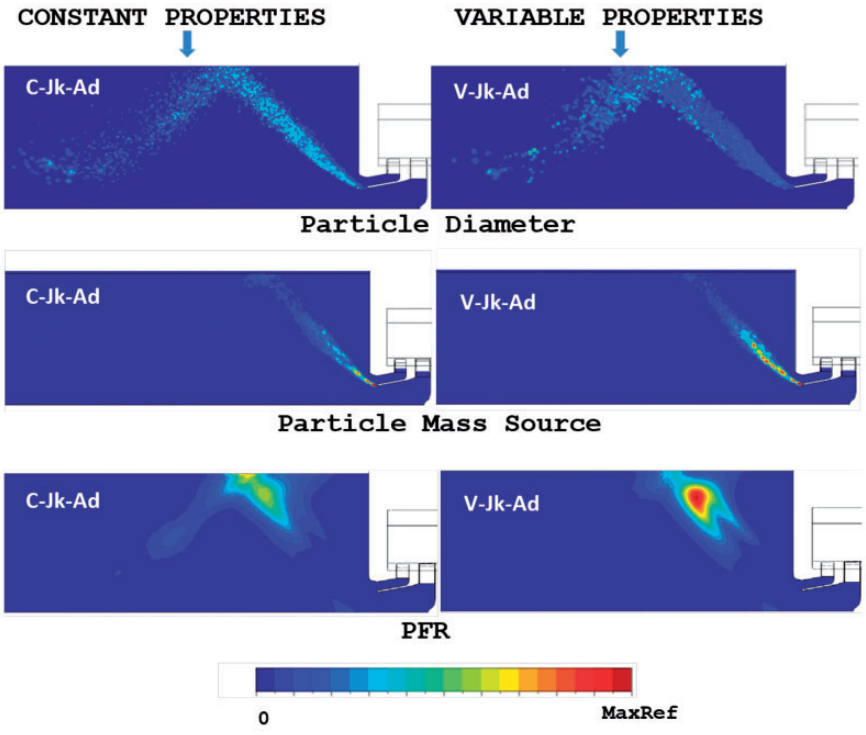

Figure 11. Contours of particle diameters, particle mass source and PFR: effect of liquid fuel properties.

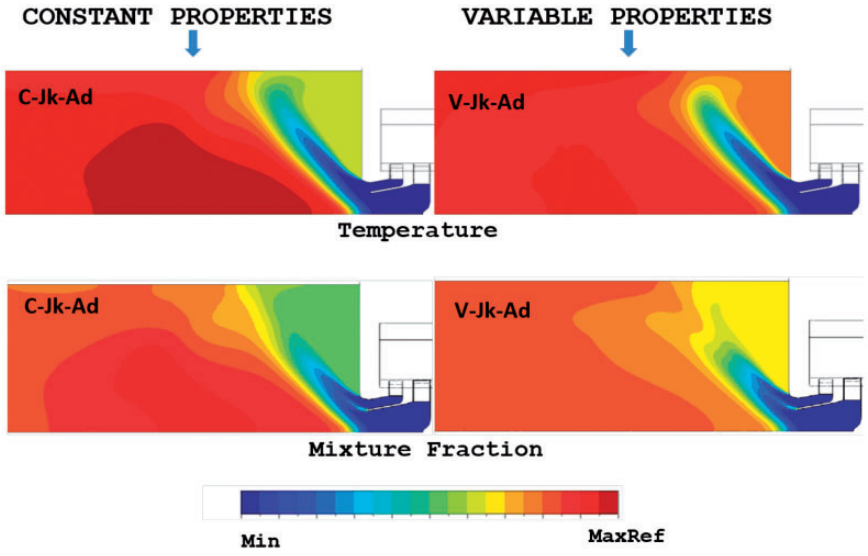

Figure 12. Contours of mixture fraction and temperature: effect of liquid fuel properties.

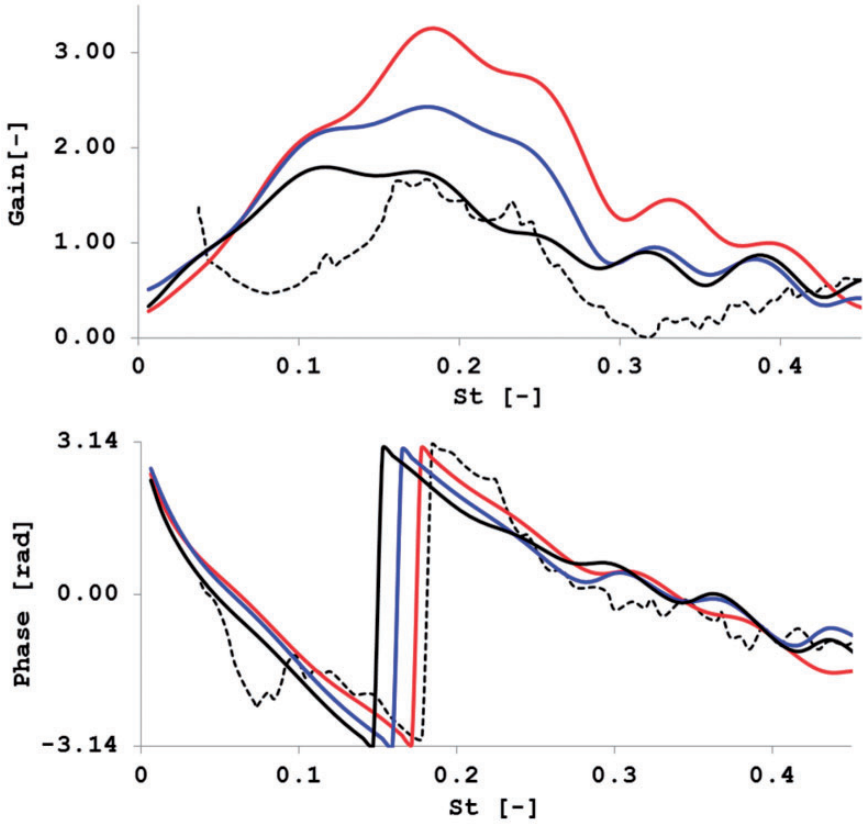

Figure 13. Experimental FTF (- -) and FTFs computed with constant (— C-Jk-Ad) and variable (— V-Jk-Ad) liquid properties with JetAk99 mechanism and FTT for the case with variable properties and JetAk99N mechanism (—; V-JkN-Ad).

the gain shows a decreasing trend, opposite to what is observed in the measurements. The low frequency range continues to show the larger discrepancies compared with experiments suggesting that the mechanism governing the flame response in this range is not represented by the CFD model.

Interestingly, the predicted phase follows correctly the experiments. Representative time lags between the

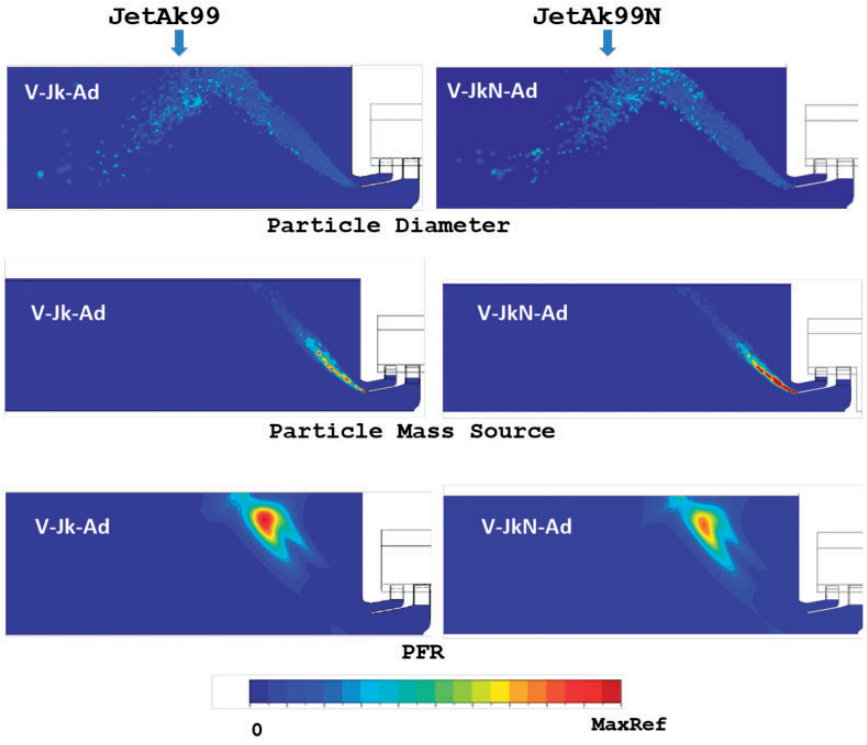

Figure 14. Effect of the chemical mechanism on particle mass source and PFR.

acoustic and heat release fluctuations are predicted but for low frequencies.

5.2. Sensitivity to chemical reaction mechanism

A further investigation has been carried out to see the role of chemical kinetics on the results.

In particular the following reaction was considered

$$C_{12}H_{23} + N_2 \rightarrow 12CH + 11H + N_2 \qquad (4)$$

whose reaction rate is expressed as:

$$\dot{\omega}_{C_{12}H_{23}} = KC^{\alpha}_{C_{12}H_{23}} C^{\beta}_{N_2} \cdot \exp\left(\frac{-E_a}{RT}\right) \qquad (5)$$

where $C_{C_{12}H_{23}}$ and C_{N_2} are the molar concentrations of JetA and nitrogen, respectively, E_a is the activation energy and K is the pre-exponential factor. This reaction is a global step which approximates the complex, fast, pyrolysis reactions of the main fuel species in the early part of the flame. This process cannot be treated as an elementary reaction and therefore its reaction order (α and β) needs to be determined from a tuning procedure against experimental or data or results obtained with a more detailed mechanism.

To explore the effect of such source of uncertainty, a sensitivity to the values of coefficients α and β is performed. Coefficients are both changed from their original value of 1.0 (JetAk99) to 0.8: this new set is hereafter named JetAk99N mechanism. This sensitivity was realized in the setup where temperature dependent liquid fuel properties are implemented.

The main effect of this modification is an increase of the global reaction rate: the results can be observed in Figures 14 and 15. The increase of the early pyrolysis reaction rate produces an increase in particle evaporation rate in the first part of the flame (see Figure 14). This leaves more time for fuel air mixing, resulting in a more homogeneous mixture in the downstream region. The final consequence is a more uniform temperature distribution with lower peak values in the corner recirculation region (see Figure 15).

The computed FTF is also plotted in Figure 13. Comparing the FTFs obtained with the two different mechanisms, a lower amplitude is predicted with the simulation adopting JetAk99N. This can be explained by observing that the flame is now spread over a larger region, with reduced peaks of PFR. The increased flame length and volume should lead to lower power density, a decrease of heat release fluctuations amplitude and therefore a reduced FTF gain.[44,45] The distance between the injector outlet plane and the PFR peak location is unchanged. Therefore, no significant differences are observed for the FTF phase.

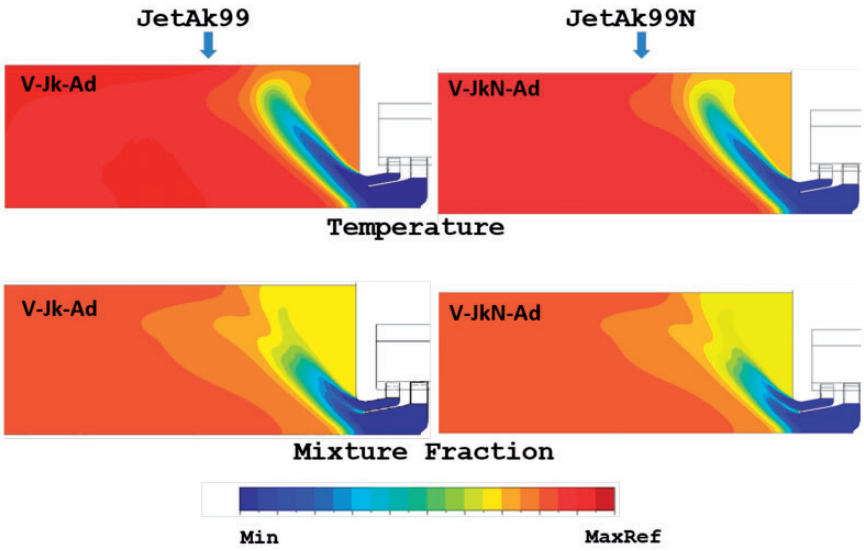

Figure 15. Effect of the chemical mechanism on mixture fraction and temperature.

5.3. Sensitivity to combustor wall temperature

The effect of the wall thermal boundary condition is investigated in this section. The simulation is performed starting from the previous set-up with the Jetk99N mechanism. A constant temperature is imposed at the combustor walls. As the actual wall temperature of the air-cooled experimental apparatus is not known a reasonable low temperature value has been assigned in order to stress the effect (600 K). In the adiabatic cases the maximum wall temperature reached is close the overall adiabatic flame temperature and it was reached near combustor outlet.

As seen in Figure 16, lower temperature levels are reached in the region close to the wall as well as in the corner recirculation where the cooler flow is transported.

The evaporation pattern is changed: a less intense evaporation is predicted in the first part, as seen in Figure 17. The peak of mass source close to the injection is decreased. The droplets' diameter reduces during the longer life-path, which continues in the recirculation region where the evaporation is completed. Therefore mass source is spread over a larger region leading to a richer inner recirculation, as seen in Figure 16. However, mixture fraction levels at the location of maximum heat release are comparable between the adiabatic and diabatic cases. The effect on PFR is limited to a shift upstream of the high intensity region, as a consequence of the inhibition of the reaction at the wall proximity.

The computed FTF is plotted in Figure 18 against experiment and the adiabatic case. The experimental trend in the first part of the domain is correctly predicted by the model despite slightly higher amplitudes. However, a general overestimation of the experiments and a wrong trend is found for higher frequency. Moreover, looking at the phase plot it is possible to see how the experimental response is not followed by the computed FTF. Probably the numerical value chosen for the wall temperature is too low and the consequent flame evolution is altered too much.

In general, the result suggests that the wall temperature can have an important role in driving low-frequency fluctuations and the low-pass filtering behaviour of the flame.

To provide a more physical insight on this effect a frequency analysis is carried out where the local dynamical flame behaviour is condensed by using fast Fourier transformation (FFT). A series of images of the heat release is exported during the acoustically excited CFD calculations used for the FTF computation.

With this technique, mainly used in experimental investigations,[46–49] a locally resolved FTF can be calculated for each node.

As for the global FTFs, a signal serves as a reference, which is especially important for the phase. In this case the velocity at the burner mouth is used as reference signal. Being a broadband signal because of the excitation imposed at the domain inlet, a filtering operation is necessary to isolate the frequency to be analysed. The images are post processed node by node and then Fourier transformed. The resulting amplitude image shows the regions of activity within the flame, with the values being proportional to the intensity oscillation amplitude at the investigated frequency. The corresponding phase image represents the phase angle in each point relative to the reference velocity signal. A combination of the former is also used colouring the picture with the product of the amplitude times

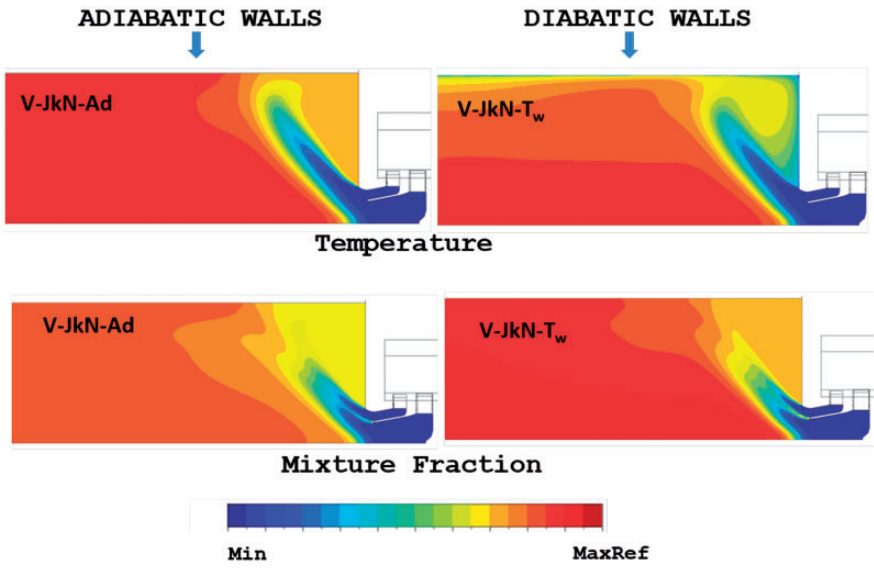

Figure 16. Mixture fraction and temperature contours in case of adiabatic and diabatic combustor walls.

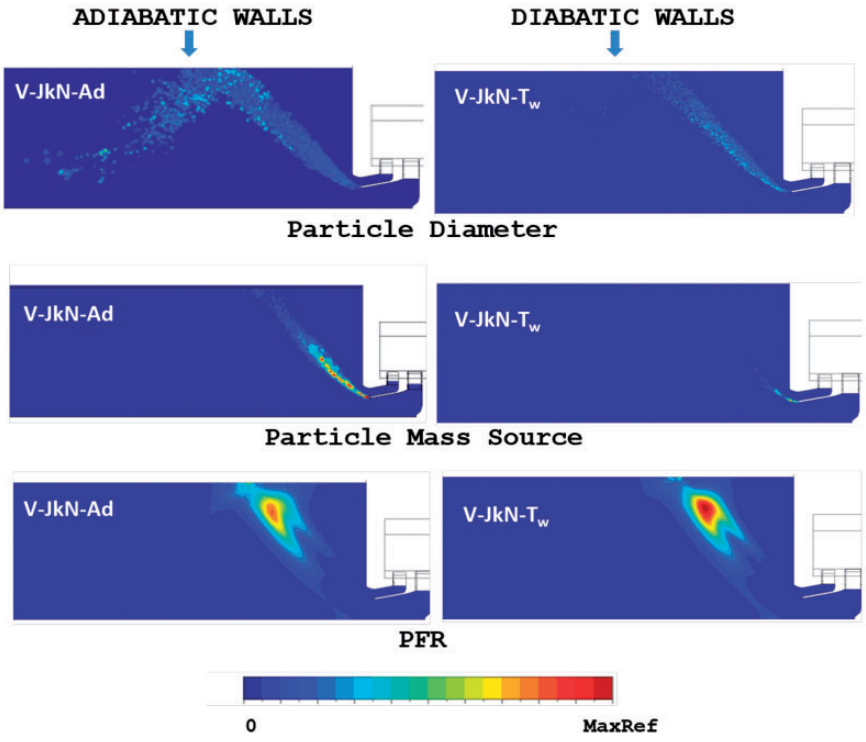

Figure 17. Droplet diameter, particle mass source and PFR for the two cases with adiabatic and diabatic combustor walls.

the sign of the phase. Such a visualization shows where the heat release oscillations are in phase with the signal, and their intensity at the same time. The operation can be repeated at different frequencies to investigate the flame response all over the frequency spectrum.

In Figure 19, the normalized heat release fluctuation amplitude, phase and the product of the former times the sign of the phase are shown for three frequencies: St = 0.03, 0.074 and 0.184.

Analysing the results some similarity can be found between the adiabatic and the diabatic cases.

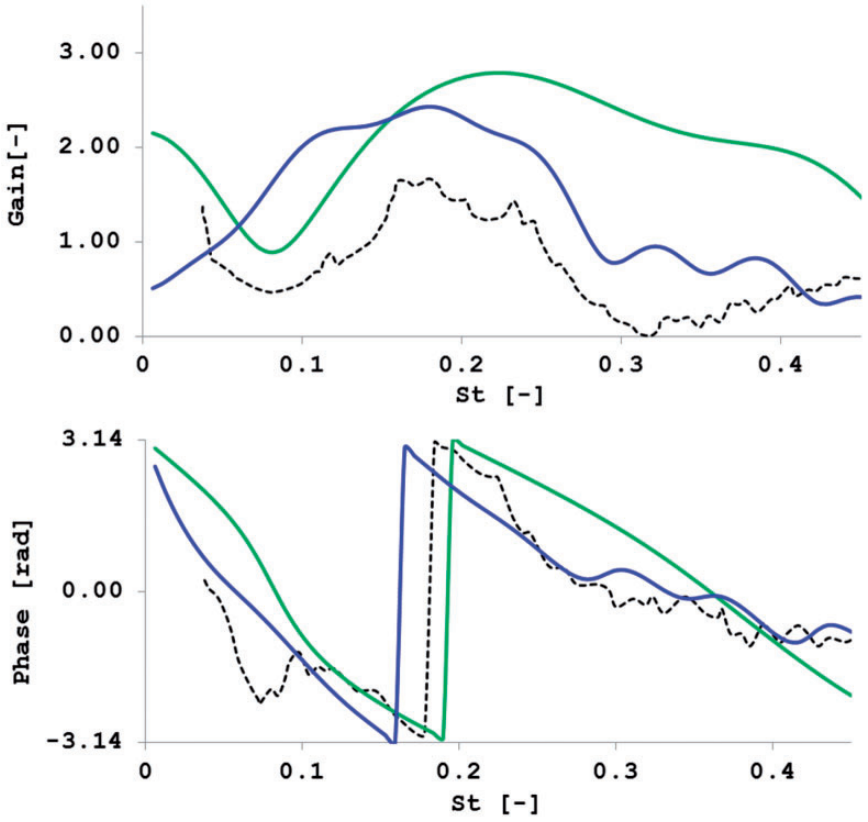

Figure 18. Flame transfer function computed with diabatic combustor walls (— V-JkN-Tw) against the adiabatic case (— V-JkN-Ad) and experiments (- -).

Comparing the results where both cases present a minimum in the FTF gain (St = 0.03 for the adiabatic case and St = 0.074 for the diabatic) similar shape and phase values are predicted. The main region of activity is coincident with the PFR peak (see Figure 17). Lower activity can be observed also along the droplet path. The phase is positive and close to π in every point, meaning that the heat release fluctuates in phase with the velocity.

Looking at those frequencies where high FTF gains are predicted (St = 0.074 and 0.184 for the adiabatic case, St = 0.03 and 0.184 for the diabatic), the active region is modified and a second peak appears at the impinging location of the droplet at the wall. A three-branch structure begins to emerge, which is fully defined at higher frequencies.

The flame fluctuates along the inner and outer shear layers but the maximum of activity is still at the tip of the flame and at the wall proximity. The bottom pictures show that the central region and the one at the combustor wall fluctuate out of phase with respect to the shear layers.

Finally, looking at the phase contours for both the flames the independent evolution of the two jets from the primary and secondary swirlers is seen. The higher the frequency, the more evident the distinction.

5.4. Final assessment through quality checks

In order to evaluate if the identified impulse response describes the relationship between the measured input signals and system responses, and if the underlying physics is correctly predicted, the Q parameter is evaluated according to Ljung.[41] This is a measure of how well the actual signal is reproduced by the model. During the SI procedure to compute the FTF only the 80–85% of the data from the exported time series are used. The remaining data are used to judge the model quality. The remaining part of the exported velocity time series is given as input to the computed model (computed FTF) whose output (the estimated q') is compared with the remaining part of the time series of heat release fluctuations coming from CFD.

Q is a measure of the area comprised within the two curves and for the simulation presented in the present work it ranged from the lowest values of around 60% to values close to 95% in other cases.

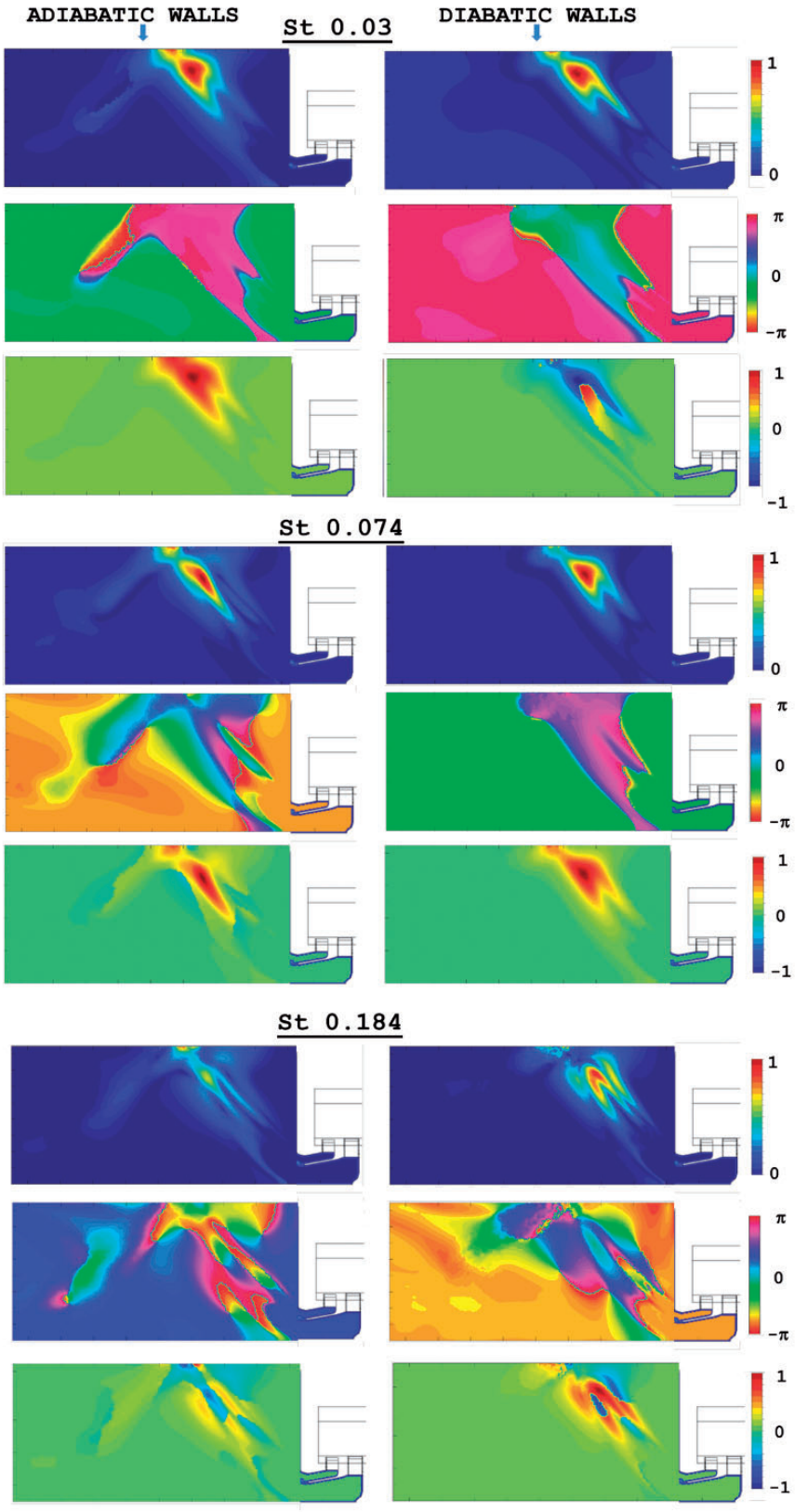

Figure 19. Normalized heat release amplitude (top), phase (centre) and amplitude times (sign(phase)) (bottom) for adiabatic and diabatic cases at St = 0.03, 0.074 and 0.184.

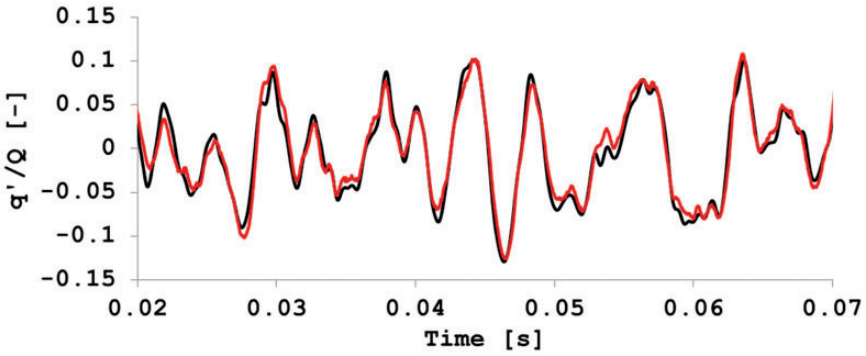

Figure 20. Comparison between the estimated output and the 'best fit'.

In Figure 20, one example of comparison between the estimated output and the 'best fit' (the output of CFD) is shown for a $Q = 90\%$ estimation.

The good quality of the results is indicative that a SISO model based on velocity at the injector outlet as input may be adequate to reproduce the global flame response as in the CFD simulation.

This means that the discrepancies between the computed FTF and the experiments are only due to an incomplete numerical modelling of the flame.

Once a numerical model is found able to reproduce with higher accuracy the complex spray flame evolution, the discussed SISO model is considered able to represent the flame dynamics and might be reasonably used to perform stability analyses of the combustor.

6. Conclusions

The dynamics of a spray flame generated by a PERM injector have been numerically studied. The CFD/SI method is used to compute the FTF.

Several sensitivities have been analysed to understand the impact of some modelling choices on the solution. Comparisons with measured FTF at the same conditions allowed a direct evaluation of the results and modelling strategies.

The treatment of liquid fuel properties as constant or variable with temperature has been found to have a direct impact on liquid fuel the evaporation location and velocity. On the FTF the main effects are seen on the values assumed by the amplitude.

A change in the chemical reaction mechanism shows similar effects.

The combustor wall thermal boundary condition has been found to have a more drastic impact.

Frequency analyses highlight the main regions of activity of the flame at the different frequencies. Higher FTF amplitude seems to occur when regions where the heat release fluctuates with opposite phase are observed. Smaller amplitudes are observed when the heat release fluctuates in phase with the reference velocity signal everywhere. It is also observed that heat release fluctuates following the liquid particles path. Therefore an accurate flame response cannot be obtained if the liquid phase evolution is not modelled accurately.

The present work constitutes a first important step in the study of PERM flame dynamics and sets the basis for future applications of the methodology to numerically compute its FTFs.

Acknowledgements

The authors wish to gratefully acknowledge LEMCOTEC Consortium for the kind permission of publishing the results herein.

Declaration of Conflicting Interests

The author(s) declared no potential conflicts of interest with respect to the research, authorship, and/or publication of this article.

Funding

The author(s) disclosed receipt of the following financial support for the research, authorship, and/or publication of this article: The work forms part of the LEMCOTEC Collaborative Project co-funded by the European Commission within the Seventh Framework Program (2007–2013) (grant number 283216).

References

1. Kern, M, Marinov, S, Habisreuther, P, et al. Characteristics of an ultra-lean swirl combustor flow by LES and comparison to measurements. In: *ASME turbo expo 2011: turbine technical conference and exposition*, Vancouver, BC, 6–10 June 2011, pp.321–330. New York: ASME.
2. Andreini A, Bianchini C, Caciolli G, et al. Multi-coupled numerical analysis of advanced lean burn injection systems. In: *ASME turbo expo 2014: turbine technical conference and exposition*, Düsseldorf, Germany, 16–20 June 2014, paper no. V04BT04A041. New York: ASME.
3. Andreini A, Caciolli G, Facchini B, et al. Experimental investigation of the flow field and the heat transfer on a

scaled cooled combustor liner with realistic swirling flow generated by a lean-burn injection system. *J Turbomach* 2015; 137: 031012.
4. Mazzei L, Andreini A, Facchini B, et al. Impact of swirl flow on combustor liner heat transfer and cooling: a numerical investigation with hybrid Reynolds-averaged Navier–Stokes large eddy simulation models. *J Eng Gas Turbines Power* 2016; 138: 051504.
5. Tong AY and Sirignano WA. Oscillatory vaporization of fuel droplets in an unstable combustor. *J Propul Power* 1989; 5: 257–261.
6. Duvvur A, Chiang CH and Sirignano WA. Oscillatory fuel droplet vaporization-driving mechanism for combustion instability. *J Propul Power* 1996; 12: 358–365.
7. Eckstein J, Freitag E, Hirsch C, Sattelmayer T, et al. Forced low-frequency spray characteristics of a generic airblast swirl diffusion burner. In: *ASME turbo expo 2003, collocated with the 2003 international joint power generation conference*, Atlanta, GA, 16–19 June 2003, pp.471–478. New York: ASME.
8. Lieuwen TC and Yang V. Combustion instabilities in gas turbine engines: operational experience, fundamental mechanisms, and modeling. *AIAA Prog Astronaut Aeronaut*, 2005; 210: 657pp.
9. Yu KH, Wilson KJ and Schadow KC. Liquid-fueled active instability suppression. *Symp Combust Proc* 1998; 27: 2039–2046.
10. De la Cruz Garcia M, Mastorakos E and Dowling AP. Investigations on the self-excited oscillations in a kerosene spray flame. *Combus Flame* 2009; 156: 374–384.
11. Andreini A, Facchini B, Giusti A, et al. Assessment of flame transfer function formulations for the thermoacoustic analysis of lean burn aero-engine combustors. *Energy Procedia* 2014; 45: 1422–1431.
12. Eckstein J and Sattelmayer T. Low-order modeling of low-frequency combustion instabilities in aeroengines. *J Propul Power* 2006; 22: 425–432.
13. Eckstein J. *On the mechanisms of combustion driven low-frequency oscillations in aero-engines*. PhD Thesis, Universität München, Germany, 2004.
14. Andreini A, Facchini B, Giusti A, et al. Thermoacoustic analysis of a full annular aero-engine lean combustor with multi-perforated liners. In: *Proceedings of the AIAA-CEAS aeroacoustic conference*, Berlin, 27–29 May 2013. Reston, VA: AIAA.
15. Andreini, A, Facchini, B, Giusti, A, Vitale, I, and Turrini, F. Thermoacoustic analysis of a full annular lean burn aero-engine combustor. In: *ASME turbo expo 2013: turbine technical conference and exposition*, San Antonio, TX, 3–7 June 2013, paper no. V01AT04A069. New York: ASME.
16. Komarek T and Polifke W. Impact of swirl fluctuations on the flame response of a perfectly premixed swirl burner. *J Eng Gas Turbines Power* 2010; 132: 061503.
17. Tay W-CL, Bomberg S, Ulhaq A, et al. Comparative validation study on identification of premixed flame transfer function. *J Eng Gas Turbines Power* 2012; 134: 021502.
18. Tay W-CL, Komarek T, Kaess R, et al. Identification of flame transfer functions from les of a premixed swirl burner. In: *ASME turbo expo 2010: power for land, sea, and air*, Glasgow, UK, 14–18 June 2010, pp.623–635. New York: ASME.
19. Huber A and Polifke W. Dynamics of practical premixed flames. Part I. Model structure and identification. *Int J Spray Combust Dyn* 2009; 1: 199–228.
20. Huber A and Polifke W. Dynamics of practical premixed flames. Part II. Identification and interpretation of cfd data. *Int J Spray Combust Dyn* 2009; 1: 229–249.
21. Innocenti A, Andreini A and Facchini B. Numerical identification of a premixed flame transfer function and sta bility analysis of a lean burn combustor. *Energy Procedia* 2015; 82: 358–365.
22. Yang Y, Noiray N, Scarpato A, et al. Numerical analysis of the dynamic flame response in alstom reheat combustion systems. In: *ASME turbo expo 2015: turbine technical conference and exposition*, Montreal, 15–19 June 2015, paper no. V04AT04A048. New York: ASME.
23. Hermeth S, Staffelbach G, Gicquel LYM, et al. LES evaluation of the effects of equivalence ratio fluctuations on the dynamic flame response in a real gas turbine combustion chamber. *Proc Combust Inst* 2013; 34: 3165–3173.
24. Innocenti A, Andreini A, Facchini B, et al. Numerical analysis of the dynamic flame response and thermo-acoustic stability of a full-annular lean partially-premixed combustor. In: *ASME turbo expo 2016: turbomachinery technical conference and exposition*, Seoul, 13–17 June 2016, paper no. V04BT04A003. New York: ASME.
25. Zhu M, Dowling AP and Bray KNC. Transfer function calculations for aeroengine combustion oscillations. *J Eng Gas Turbines Power* 2005; 127: 18–26.
26. Gikadi J and Sattelmayer T. Experimental determination of flame transfer function. Report no. d2.2.1. KIAI EU Project, 2013.
27. Munjal ML and Doige AG. Theory of a two source-location method for direct experimental evaluation of the four-pole parameters of an aeroacoustic element. *J Sound Vib* 1990; 141: 323–333.
28. Gikadi J. *Prediction of acoustic modes in combustors using linearized Navier–Stokes equations in frequency space*. PhD thesis, Universität München, Germany, 2013.
29. Kundu KP, Penko PF and VanOverbeke TJ. A practical mechanism for computing combustion in gas turbine engines. In: *35th joint propulsion conference and exhibit*, Los Angeles, 20–24 June 1999, p.2218. Reston, VA: AIAA.
30. Donini A, Bastiaans RJM, van Oijen JA, et al. The implementation of five-dimensional fgm combustion model for the simulation of a gas turbine model combustor. In: *ASME turbo expo 2015: turbine technical conference and exposition*, Montreal, 15–19 June 2015, paper no. V04AT04A007. New York: ASME.
31. Morsi SAJ and Alexander AJ. An investigation of particle trajectories in two-phase flow systems. *J Fluid Mech* 1972; 55: 193–208.
32. Joseph DD, Belanger J and Beavers GS. Breakup of a liquid drop suddenly exposed to a high-speed airstream. *Int J Multiphase Flow* 1999; 25: 1263–1303.
33. Gosman AD and Ioannides E. Aspects of computer simulation of liquid-fueled combustors. *J Energy* 1983; 7: 482–490.

34. Abramzon B and Sirignano WA. Droplet vaporization model for spray combustion calculations. *Int J Heat Mass Transfer* 1989; 32: 1605–1618.
35. Sazhin SS. Advanced models of fuel droplet heating and evaporation. *Prog Energy Combust Sci* 2006; 32: 162–214.
36. Hubbard GL, Denny VE and Mills AF. Droplet evaporation: effects of transients and variable properties. *Int J Heat Mass Transfer* 1975; 18: 1003–1008.
37. Rachner, M. Die Stoffeigenschaften von Kerosin Jet A-1. DLR-Mitteilung. 98-01, 152 S, 1998.
38. ANSYS. *Fluent 15.0 theory guide*. ANSYS, 2014.
39. Blumenthal RS, Subramanian P, Sujith RI, et al. Novel perspectives on the dynamics of premixed flames. *Combust Flame* 2013; 160: 1215–1224.
40. Jaensch, S, Emmert, T, Silva, CF, and Polifke, W. A grey-box identification approach for thermoacoustic network models. In: *ASME turbo expo 2014: turbine technical conference and exposition*, Düsseldorf, Germany, 16–20 June 2014, paper no. V04BT04A051. New York: ASME.
41. Ljung L. *System identification*. Berlin: Springer, 1998.
42. Andreini A, Facchini B, Innocenti A, et al. Flame transfer function identification and thermoacoustic analysis of an annular heavy-duty gas turbine combustor. In: *22nd International Congress on Sound and Vibrations*, Florence, Italy, 12–16 July 2015. International Institute of Acoustics and Vibration (IIAV) and Associazione Italiana di Acustica (AIA).
43. Polifke W and Lawn C. On the low-frequency limit of flame transfer functions. *Combust Flame* 2007; 151: 437–451.
44. Bade S, Wagner M, Hirsch C, et al. Design for thermoacoustic stability: procedure and database. *J Eng Gas Turbines Power* 2013; 135: 121507.
45. Bade S, Wagner M, Hirsch C, et al. Influence of fuel–air mixing on flame dynamics of premixed swirl burners. In: *ASME turbo expo 2014: turbine technical conference and exposition*, Düsseldorf, Germany, 16–20 June 2014, paper no. V04AT04A023. New York, ASME.
46. Freitag, E. *On the measurement and modelling of flame transfer functions at elevated pressure*. PhD Thesis, Universität München, Germany, 2009.
47. Auer MP, Hirsch T and Sattelmayer T. Influence of air and fuel mass flow fluctuations in a premix swirl burner on flame dynamics. ASME paper GT-2006-90127, 2006.
48. De Rosa AJ, Peluso SJ, Quay, BD, et al. The effect of confinement on the structure and dynamic response of lean-premixed, swirl-stabilized flames. In: *ASME turbo expo 2015: turbine technical conference and exposition*, Montreal, 15–19 June 2015, paper no. V04AT04A017. New York: ASME.
49. De Rosa AJ, Samarasinghe J, Peluso SJ, et al. Flame area fluctuation measurements in velocity-forced premixed gas turbine flames. In: *ASME turbo expo 2015: turbine technical conference and exposition*, Montreal, 15–19 June 2015, paper no. V04AT04A039. New York: ASME.